University of
Strathclyde
Glasgow

# Strathprints Institutional Repository

http://strathprints.strath.ac.uk/

# Spatial interference from well-separated split condensates

M. E. Zawadzki, P. F. Griffin, E. Riis, and A. S. Arnold[*]

*SUPA, Department of Physics, University of Strathclyde, Glasgow G4 0NG, United Kingdom*[†]

We use magnetic levitation and a variable-separation dual optical plug to obtain clear spatial interference between two condensates axially separated by up to 0.25 mm—the largest separation observed with this kind of interferometer. Clear planar fringes are observed using standard (i.e., nontomographic) resonant absorption imaging. The effect of a weak inverted parabola potential on fringe separation is observed and agrees well with theory.

## I. INTRODUCTION

It has been more than a decade since Andrews and co-workers' [1] impressive demonstration of the wavelike nature of coherent matter via the spatial interference of $^{23}$Na Bose-Einstein condensates (BECs). Such matter-wave interference experiments are of great interest for applications in ultraprecise interferometry [2] and should lead to drastic improvements in measurements of fundamental constants as well as temporal, gravitational, and rotational sensing. Here we obtain spatial BEC interference that promises significant potential for improved measurements. We use a magnetic levitation field [3] to spatially interfere two atomic clouds with relatively large spatial separations of 0.25 mm. Moreover, we use an atomic species, $^{87}$Rb, with four times the mass used in Ref. [1] and, hence, a four times smaller de Broglie wavelength for the same atomic velocities. We find tomographic imaging [1] is not required, and standard absorption imaging suffices for good-contrast 60% (30%) interference at separations of 60 $\mu$m (250 $\mu$m). We also identify a clear relationship between the interference fringe period and the magnetic levitation time in an inverted parabola trap potential.

Experiments on atomic interference have developed rapidly in the last decade and it is now possible to interfere single particles in quantum walks using the relative population of atoms in a particular state [4]. A Ramsey-type BEC interferometer using Bragg scattering has also obtained the largest time-integrated separation in condensate interference experiments [5]. Similar advances have so far been unobtainable with "Young-type" spatial interference patterns, in which the de Broglie waves of two expanding wave packets, initially spatially separate, give rise to the interference. Condensate wave function irregularities and vortices are observable only with such spatial interferometers. Recently radial splitting of condensates [6] using rf dressed potentials [7] has become popular [Fig. 1(a)], as high-contrast spatial interference fringes can be obtained due to the "point source"–like properties of the condensates when viewed along the BEC axis. Note, however, that in the radial splitting geometry, typical chip BECs can only yield interference patterns for split distances up to 26 $\mu$m [8] or times of about 400 ms (for 9-$\mu$m separation) [9]. Here we split our cigar-shaped BEC with a far-detuned optical dipole laser beam that propagates perpendicular to the BEC's

longitudinal axis [Fig. 1(b)], a geometry similar to that in Ref. [1], where interference from 40-$\mu$m BEC separation was obtained. We use a dual optical plug [Fig. 1(c)] to extend our condensate separation from 60 to 250 $\mu$m and back, observing a visibility of 30% after an experimental time of 300 ms.

It should be stressed that if two independent condensates are formed (as in this experiment), or the splitting period is too long relative to the difference in chemical potentials of the two condensates, then the interference pattern has a random phase [1,8]. For practical interferometric applications a single condensate must be smoothly split into two condensates with a fixed relative phase [6,9,16]. In future we intend to extend our proof-of-principle interferometry into the phase-coherent regime.

## II. EXPERIMENT

The BEC was created in the experimental setup described in detail in Ref. [10]. Our Ioffe-Pritchard magnetic trap has frequencies of 10 and 108 Hz in the axial and radial direction, respectively. Atoms are trapped in the $|F = 2, m_F = 2\rangle$ trapping state, with a 40-s magnetic trap lifetime and $5 \times 10^5$ atoms in a pure BEC. The condensate creation and manipulation were observed by standard absorption imaging. The imaging beam propagated perpendicular to the BEC axis and a 2× beam expander was used for imaging onto an Andor Luca CCD camera. The size of individual pixels is 10 $\mu$m, corresponding to 5 $\mu$m at the BEC's location.
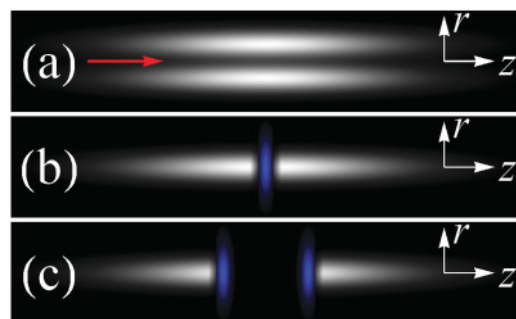


FIG. 1. (Color online) Schematic illustrating different BEC splitting geometries: (a) radial splitting using, e.g., rf dressed potentials [(red) arrow at left indicates imaging direction for fringe observation]; (b) axial splitting using a blue-detuned dipole beam; (c) the variable-separation axial splitting using dual dipole beams reported on in this paper.

[*]a.arnold@phys.strath.ac.uk

[†]URL: www.photonics.phys.strath.ac.uk/AtomOptics/

043608-1

Our dipole beam is generated by 50 mW of light from a free-running 658-nm diode laser, far to the blue of the Rb $D_2$ resonance at 780 nm. To create a high-intensity dipole beam we used an 80-mm-focal-length achromat lens. The elliptical diode laser beam shape was focused to beam waists of 8.8 and 13.7 $\mu$m in the axial and radial direction, respectively. This yields a maximum potential of 30 $\mu$K that completely isolates split condensates from each other, and tunneling effects can be neglected. The dipole beam allows fully coherent and adiabatic splitting of the BEC, with an estimated condensate photon scattering rate of 1 mHz per atom. The alignment of the dipole potential was facilitated by combining the 658-nm beam with a "tracer" 780-nm repump ($F = 1 \rightarrow F' = 2$) beam [11] on a beam splitter to create a copropagating beam with a much higher scattering rate and optical potential. For all experiments in this paper the dipole beam was on throughout evaporative cooling to BECs—resulting in the creation of two independent samples of coherent matter with a random relative phase.

As acousto-optical modulators (AOMs) can vary the deflection angle and beam intensity of a dipole beam via the applied rf and power, respectively, they are a useful tool for creating arbitrary patterns in BEC experiments through the time-averaged optical dipole potential [12–14]. However, their use with BECs has largely been through red-detuned light, although blue-detuned potentials [15] offer substantially lower decoherence rates.

### III. DUAL OPTICAL PLUG

We split our blue-detuned dipole laser beam into two beams, with variable separation, via an 80-MHz AOM. As the first-order beam from an AOM is deflected proportionally to the rf drive frequency, if we use an rf spectrum consisting of multiple spectral components we can form multiple simultaneous beams [16]. Our adiabatic splitting is induced by dipole beam sidebands driven by amplitude modulation of the rf carrier frequency fed to the AOM. The amplitude modulation is obtained by mixing two frequencies, a stable carrier frequency $\nu_0 = 80$ MHz and a variable frequency modulation signal $0 < \nu_{mod} < 20$ MHz, yielding two tunable sidebands at $\nu = \nu_0 \pm \nu_{mod}$. The rf modulation frequency comes from a computer-controlled synthesized signal generator. A standard double-balanced mixer is used to mix the signal and carrier rf signals. The decrease in amplitude of the carrier frequency from the sidebands is of order 40 dB, and the carrier frequency dipole beam has a negligible effect on the atoms. The linear response of the rf drive frequency to beam deflection results in two beams at relative deflection angles $\delta\theta = \pm 2.5$ mrad for a 20-MHz modulation frequency.

For low modulation frequencies, the two dipole beams have a good spatial overlap, effectively resulting in a single beam with a beat phenomenon at the modulation frequency; that is, the beam intensity varies in brightness sinusoidally in time with period $T = 1/(2\nu_{mod})$. To highlight the low heating rate of blue detuned light, we used this beating to perform an experiment similar to that in Ref. [13]: we studied heating as a function of intensity modulation frequency of the dipole beam during evaporation to a BEC. Heating was observed as the fraction of the BEC lost after rf evaporation in a double-well potential composed of the magnetic trap with a
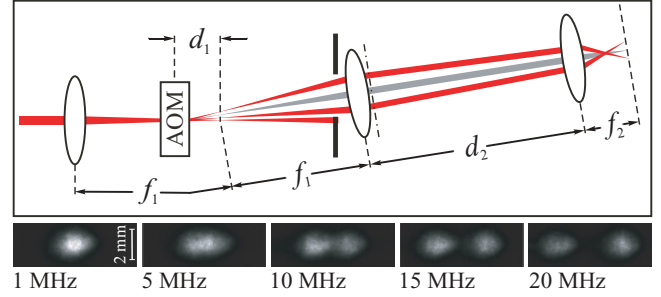


FIG. 2. (Color online) The 658-nm dipole beam path for splitting the BEC. The acousto-optical modulator (AOM) was offset by a distance $d_1$ from the focal point of the $1\times$ beam expander to enable output beam deflection at the beam waist after the final lens. The modulated rf carrier frequency results in two rf sidebands and a suppressed carrier, resulting in two optical beams with spatial separation determined by the rf modulation frequency as shown in the experimental beam image series.

dipole beam that had a sinusoidally modulated intensity. The main result was that no heating was observed for modulation rates greater than 1 kHz, a limit significantly lower than the 30–40 kHz in Ref. [13]. In principle the trap might be adiabatically deformable at modulation frequencies less than 1 kHz, however, because of atomic motion in the harmonic magnetic trap, care would then need to be taken that the trap modulation does not interfere with evaporation.

The position of our AOM (Fig. 2) was offset by a distance $d_1 = 10$ cm from the focal point of a $1\times$ beam expander comprised of two planoconvex lenses with $f_1 = 25$ cm focal length. After a (noncritical) propagation distance $d_2$ the beams are focused by an achromat lens with focal length $f_2 = 8$ cm. Using standard paraxial $ABCD$ matrices one can show that the waist after the $f_2$ lens yields beam displacements $\delta z = d_1 f_2 \delta\theta / f_1 = \pm 80$ $\mu$m for a modulation frequency of 20 MHz (Fig. 2). Although the rf power in the sidebands is constant, a small drop in the optical power of the beams is observable at large displacements due to reduced AOM diffraction efficiency. The largest achievable center-of-mass (c.m.) separation of two BECs by the repulsive potential of the dipole beams was 250 $\mu$m, with spatial interference between separated condensates still clearly observable. We believe this is the largest splitting observed in a "Young-type" spatial BEC interferometer.

### IV. FRINGES

The anisotropic character of a cigar-shaped Ioffe-Pritchard trap leads to two different expansion velocities, as the mean-field forces from a repulsive BEC are proportional to the condensate's density gradient; hence the expansion velocity is much greater in the radial direction than the axial direction. Moreover, using a dipole beam to create a macroscopic axial separation of our matter waves, we need a concomitantly longer expansion time for BEC recombination and interference than is required for radially split BECs [6].

The fringe spacing $\lambda$ arises from the de Broglie waves of two condensates and takes the familiar form:

$$\lambda = h/(mv), \quad (1)$$

where $h$ is Planck's constant, $m$ is the atomic mass, and $v = d/t$ is the *relative* speed between two pointlike condensates as a function of their c.m. separation $d$ and expansion time $t$. The duration of ballistic expansion in free fall is usually limited by the size of the imaging area and the dimensions of the BEC vacuum cell: times of about 100 ms lead to long drops of 49 mm, and the corresponding condensate speed of 1 m/s leads to blurred images. To eliminate the inconvenience of gravity, a "levitation" field can be used [3] whereby a magnetic field gradient counteracts the gravitational acceleration. The levitation field keeps the atoms in the region of interest for time intervals ($t > 80$ ms) that are long enough to make our interference pattern optically resolvable.

Our levitation field is provided by the existing four circular coils that form the toroidal quadrupole field [10] of our ring Ioffe-Pritchard trap. The levitation mechanism uses the weak-field-seeking $|2, 2\rangle$ atoms of the BEC, which are attracted to the local field minimum. After creation of a BEC in the magnetic trap by a 25-s evaporative cooling cycle, "antigravity" conditions are obtained with a vertical gradient of 15 G/cm. An additional vertical constant field is added to the quadrupole magnetic field to reduce lensing [17] in the vertical and imaging directions.
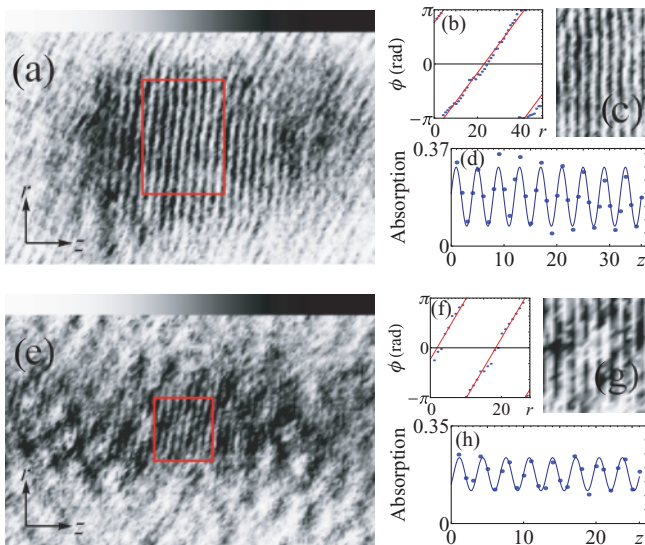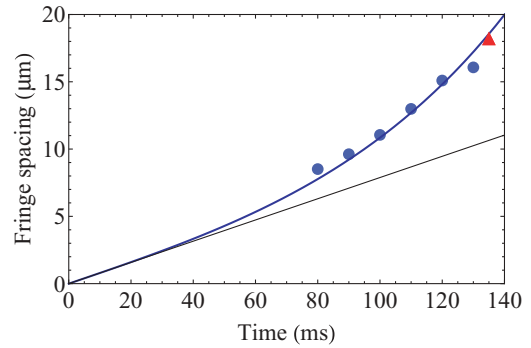


FIG. 4. (Color online) Fringe spacing as a function of levitation time. Ballistic expansion theory for $d = 60$ $\mu$m-separated BECs [diagonal (black) line] and experimental data (circles) are shown, as well as a [thick (blue)] $\sinh(\omega t)/\omega$ curve using $\omega = 14$ rad/s (a geometrical ring property), which has a $d = 60$ $\mu$m fit. The model aptly represents the fringe spacing in an inverted parabolic potential. The triangle was derived from the image Fig. 3(a).

Figure 3(a) represents an example of the high-contrast (60%) interference pattern when two BEC clouds were originally separated by 60 $\mu$m (c.m. distance) with a single optical plug, then recombined using the levitation magnetic field. Standard (i.e., nontomographic [1]) absorption imaging is used. The interference pattern when the BEC is split from a c.m. separation of 60 $\mu$m to one of 250 $\mu$m over 80 ms, returned to 60-$\mu$m separation over 80 ms, and then levitated for 150 ms has clear continuous spatial fringes with 30% contrast [Fig. 3(e)]. To straighten our experimental fringes we first obtain, for each image row, the phase of the Fourier component associated with the fringes [Figs. 3(b) and 3(f)]. We then apply a linear phase fit across all rows of the Fourier transform, before inverse Fourier transforming to obtain the images shown in Figs. 3(c) and 3(g). By averaging these corrected images over all rows, removing the background, and fitting sine curves to the experimental data, we obtain the fringes and their contrast [Figs. 3(d) and 3(h)].

Our BEC is levitated in an axial potential that is approximately an inverted parabola, $U_z = -m\omega^2 z^2/2$, due to



FIG. 3. (Color online) Interference patterns ($0.8 \times 0.5$ mm$^2$) for (a) 60-$\mu$m-separated BECs and (e) BECs split 60 $\mu$m–250 $\mu$m–60 $\mu$m over a 160-ms period. In both cases the pictures were taken after a further 135 ms of magnetic levitation, which, for (a), corresponds to the triangle in Fig. 4. The phases of the Fourier components of the fringes for the selected areas in the (red) boxes in (a) and (e) can be obtained [(blue) points in (b) and (f)] and fit with a sawtooth linear phase shift [(red) curves in (b) and (f)]. These sawtooth phase corrections can then be applied to the Fourier transform, before performing the inverse transform shown in (c) and (g). These corrected images can then be averaged over the image rows to obtain the (blue) circles in (d) and (h), with their sinusoidal fits [(blue) curves]. Absorption is measured using the natural logarithm. Each row or column (i.e., pixel) corresponds to $5 \times 5$ $\mu$m$^2$. The fringe period in (e) is shorter than in (a), as the condensates have a residual counterpropagating velocity after the 250 $\mu$m → 60 $\mu$m separation phase.
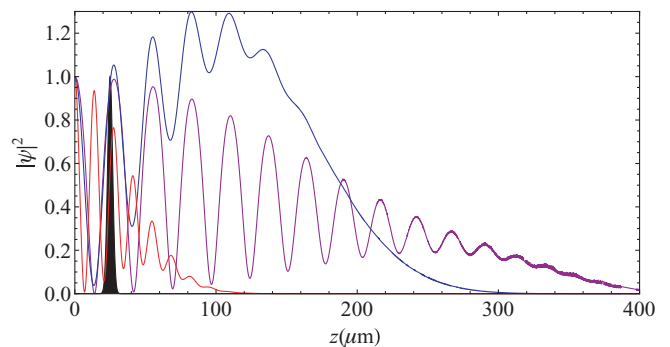


FIG. 5. (Color online) Relative theoretical probability distributions (fringes; with even symmetry about $z = 0$) obtained when two Gaussian initial wave packets (black) are released for 150 ms in a potential: $U_z = 0$ (red) and $U_z = -m\omega^2 z^2/2$ (blue and purple curves). Interatomic repulsion is either absent (red and blue curves) or present (purple curve). Increasing the nonlinear term in the Schrödinger equation affects the width of the final distribution but not the fringe period.

the circular nature of our toroidal quadrupole field. The magnitude of $\omega$ corresponds to that of a rigid pendulum, that is, $\omega = g/r = 14$ rad/s, where $g$ is the acceleration due to gravity and $r = 5$ cm is the radius of our ring. By solving the one-dimensional, time-dependent, Schrödinger equation (with and without a nonlinear interatomic repulsion), one can show that the fringe spacing in the potential $U_z$ is modified from Eq. (1) to $\lambda' = \lambda \sinh(\omega t)/\omega$. This interference fringe spacing dependence on the levitation potential is clearly observable in the experimental fringe periodicity (Fig. 4). Theory also clearly shows that the fringe spacing is not altered by interatomic repulsion (Fig. 5). Interestingly the fringe separation has a similar dependence to that attributed to interatomic repulsion in interferometry experiments on a chip, albeit at a higher atomic density [6].

## V. CONCLUSIONS

The creation of spatial interference between split BECs with macroscopic separation offers a promising outlook for future atom interferometry-based measurements, for example, our degenerate gas experiments in macroscopic ring geometries [10]. We intend to extend our proof-of-principle experiments and perform interferometry with a controlled phase by forming condensates with a weak link (due to a lower dipole beam power) and raising the barrier between condensates immediately before interferometric experiments. We will also carry out experiments with the plug's rf spectrum altered to create BECs in multiple wells—an "optical fork" for BECs, toward the limit of a one-dimensional optical lattice with dynamic spacing. A weak carrier and small separation between dipole beams will also allow the formation of a three-well BEC, ideal for STIRAP experiments [18] transferring a BEC from the left quantum well (say) to the right quantum well, effectively bypassing the second quantum well.

[1] M. R. Andrews, C. G. Townsend, H.-J. Miesner, D. S. Durfee, D. M. Kurn, and W. Ketterle, Science **275**, 637 (1997).

[2] T. L. Gustavson, P. Bouyer, and M. A. Kasevich, Phys. Rev. Lett. **78**, 2046 (1997); S. Gupta, K. Dieckmann, Z. Hadzibabic, and D. E. Pritchard, *ibid.* **89**, 140401 (2002); Y.-J. Wang, D. Z. Anderson, V. M. Bright, E. A. Cornell, Q. Diot, T. Kishimoto, M. Prentiss, R. A. Saravanan, S. R. Segal, and S. Wu, *ibid.* **94**, 090405 (2005).

[3] M. H. Anderson, J. R. Ensher, M. R. Matthews, C. E. Wieman, and E. A. Cornell, Science **269**, 198 (1995); D. J. Han, M. T. DePue, and D. S. Weiss, Phys. Rev. A **63**, 023405 (2001); T. Weber, J. Herbig, M. Mark, H.-C. Nägerl, and R. Grimm, Science **299**, 232 (2003).

[4] H. Schmitz, R. Matjeschk, Ch. Schneider, J. Glueckert, M. Enderlein, T. Huber, and T. Schaetz, Phys. Rev. Lett. **103**, 090504 (2009); M. Karski, L. Förster, J.-Min. Choi, A. Steffen, W. Alt, D. Meschede, and A. Widera, Science **325**, 174 (2009).

[5] O. Garcia, B. Deissler, K. J. Hughes, J. M. Reeves, and C. A. Sackett, Phys. Rev. A **74**, 031601(R) (2006); J. H. T. Burke, B. Deissler, K. J. Hughes, and C. A. Sackett, *ibid.* **78**, 023619 (2008).

[6] T. Schumm, S. Hofferberth, L. M. Andersson, S. Wildermuth, S. Groth, I. Bar-Joseph, J. Schmiedmayer, and P. Krüger, Nature Phys. **1**, 57 (2005).

[7] O. Zobay and B. M. Garraway, Phys. Rev. Lett. **86**, 1195 (2001); Y. Colombe, E. Knyazchyan, O. Morizot, B. Mercier, V. Lorent, and H. Perrin, Europhys. Lett. **67**, 593 (2004).

[8] Y. Shin, C. Sanner, G.-B. Jo, T. A. Pasquini, M. Saba, W. Ketterle, D. E. Pritchard, M. Vengalattore, and M. Prentiss, Phys. Rev. A **72**, 021604(R) (2005).

[9] G.-B. Jo, Y. Shin, S. Will, T. A. Pasquini, M. Saba, W. Ketterle, D. E. Pritchard, M. Vengalattore, and M. Prentiss, Phys. Rev. Lett. **98**, 030407 (2007).

[10] A. S. Arnold, C. S. Garvie, and E. Riis, Phys. Rev. A **73**, 041606(R) (2006); P. F. Griffin, E. Riis, and A. S. Arnold, *ibid.* **77**, 051402(R) (2008).

[11] K. M. O'Hara, S. R. Granade, M. E. Gehm, T. A. Savard, S. Bali, C. Freed, and J. E. Thomas, Phys. Rev. Lett. **82**, 4204 (1999).

[12] R. Onofrio, D. S. Durfee, C. Raman, M. Köhl, C. E. Kuklewicz, and W. Ketterle, Phys. Rev. Lett. **84**, 810 (2000).

[13] S. K. Schnelle, E. D. van Ooijen, M. J. Davis, N. R. Heckenberg, and H. Rubinsztein-Dunlop, Opt. Express **16**, 1405 (2008).

[14] K. Henderson, C. Ryu, C. MacCormick, and M. G. Boshier, New J. Phys. **11**, 043030 (2009).

[15] N. Houston, E. Riis, and A. S. Arnold, J. Phys. B **41**, 211001 (2008).

[16] Y. Shin, M. Saba, T. A. Pasquini, W. Ketterle, D. E. Pritchard, and A. E. Leanhardt, Phys. Rev. Lett. **92**, 050405 (2004).

[17] I. Bloch, M. Köhl, M. Greiner, T. W. Hänsch, and T. Esslinger, Phys. Rev. Lett. **87**, 030401 (2001); A. S. Arnold, C. Mac-Cormick, and M. G. Boshier, Phys. Rev. A **65**, 031601(R) (2002); J. Phys. B **37**, 485 (2004); M. Köhl, Th. Busch, K. Mølmer, T. W. Hänsch, and T. Esslinger, Phys. Rev. A **72**, 063618 (2005).

[18] M. Rab, J. H. Cole, N. G. Parker, A. D. Greentree, L. C. L. Hollenberg, and A. M. Martin, Phys. Rev. A **77**, 061602(R) (2008).